Discrete elements for 3D microfluidics

Krisna C. Bhargava[a], Bryant Thompson[b], and Noah Malmstadt[a,1]

[a]Mork Family Department of Chemical Engineering and Materials Science and [b]Department of Biomedical Engineering, University of Southern California, Los Angeles, CA 90089

Edited by David A. Weitz, Harvard University, Cambridge, MA, and approved August 21, 2014 (received for review August 2, 2014)

Microfluidic systems are rapidly becoming commonplace tools for high-precision materials synthesis, biochemical sample preparation, and biophysical analysis. Typically, microfluidic systems are constructed in monolithic form by means of microfabrication and, increasingly, by additive techniques. These methods restrict the design and assembly of truly complex systems by placing unnecessary emphasis on complete functional integration of operational elements in a planar environment. Here, we present a solution based on discrete elements that liberates designers to build large-scale microfluidic systems in three dimensions that are modular, diverse, and predictable by simple network analysis techniques. We develop a sample library of standardized components and connectors manufactured using stereolithography. We predict and validate the flow characteristics of these individual components to design and construct a tunable concentration gradient generator with a scalable number of parallel outputs. We show that these systems are rapidly reconfigurable by constructing three variations of a device for generating monodisperse microdroplets in two distinct size regimes and in a high-throughput mode by simple replacement of emulsifier subcircuits. Finally, we demonstrate the capability for active process monitoring by constructing an optical sensing element for detecting water droplets in a fluorocarbon stream and quantifying their size and frequency. By moving away from large-scale integration toward standardized discrete elements, we demonstrate the potential to reduce the practice of designing and assembling complex 3D microfluidic circuits to a methodology comparable to that found in the electronics industry.

modular microfluidics | microfluidic circuit design | 3D-printed microfluidics

Microfluidic technology has been broadly applied in domains including biochemical analysis, fundamental biomedical research, analytical chemistry, and materials synthesis (1–5). The advancement of this field has been driven by the adaptation of microfabrication technologies developed for semiconductor electronics fabrication. Modern microfluidic systems have therefore followed in the footsteps of microelectronics by placing an emphasis on functional complexity and total integration. However, while the demands of signal processing and computation naturally imply the need for greater levels of monolithic integration in electronic systems, many microfluidic applications require a different sort of intricacy than is natural to 2D (or layered 2D) environments. For example, routing channels in systems where multiple fluid streams must be handled is a significant design challenge for technologies limited to planar substrates. In addition, as the number of fluidic operations per device increases, the space requirements on a micromachined surface also increase, leading to a disproportionate increase in manufacturing cost and difficulty.

In this report, we describe an approach to microfluidic device design based on discrete elements that can be easily assembled to create complex, modular, and robust circuits in three dimensions. Analogous to the use of discrete components with standardized interconnect footprints in electronics design, the devices described here are connected in a self-aligned manner and held together reversibly. Components are fabricated using high-precision additive manufacturing techniques, giving a great deal of freedom in designing their individual hydrodynamic characteristics and enabling the application of circuit theory and network analysis to system modeling. We envision a design paradigm in which engineers select parts from a library of standardized active and passive components and then assemble these parts on a benchtop free of the constraints and difficulties of clean-room processing.

Using discrete components to construct microfluidic circuits offers several advantages over traditional methods with respect to system cost, planning, and maintenance. In general, two modular microfluidic design strategies have been proposed previously: systems analogous to electronic breadboards (6, 7) and interconnected monolithic chips (8–10). Burns and coworkers demonstrated a variation to breadboard-style systems by fabricating planar microfluidic puzzle pieces with self-aligning channels (11, 12). Several industrial manufacturers of standard microfluidic integrated circuits offer products which use system-specific chip-to-chip and chip-to-world interconnects (*SI Text*, *Note S1*). While these solutions promise to expedite the development cycle, they rely on relatively costly and time-consuming microfabrication processes, they don't generally allow nonplanar microfluidic circuit design, and they inherently prohibit designers from customizing circuits at an elemental level.

The hydraulic analogy to electronic circuits provides that pressure-driven, low Reynolds Number flow of an incompressible fluid can be analyzed using Kirchoff's Laws, enabling the determination of pressure–flow rate relationships in a complex system based on nodal and mesh techniques (13). In most microfluidic applications, the primary function of the device can be specified by a set of intended flow rates, pressure gradients, mixing or dilution ratios, or some combination thereof. In electronic circuit design, analogous specifications are often referred to as "load requirements" to which the designer adapts their election of a circuit topology and selection of standardized parts. While some efforts have been made toward simplifying the microfluidic system design

Significance

Microfluidic systems promise to improve the analysis and synthesis of materials, biological or otherwise, by lowering the required volume of fluid samples, offering a tightly controlled fluid-handling environment, and simultaneously integrating various chemical processes. To build these systems, designers depend on microfabrication techniques that restrict them to arranging their designs in two dimensions and completely fabricating their design in a single step. This study introduces modular, reconfigurable components containing fluidic and sensor elements adaptable to many different microfluidic circuits. These elements can be assembled to allow for 3D routing of channels. This assembly approach allows for the application of network analysis techniques like those used in classical electronic circuit design, facilitating the straightforward design of predictable flow systems.

Author contributions: K.C.B., B.T., and N.M. designed research; K.C.B. and B.T. performed research; K.C.B., B.T., and N.M. analyzed data; and K.C.B., B.T., and N.M. wrote the paper.

Conflict of interest statement: A patent has been filed by the Stevens Center for Innovation at the University of Southern California on the reported approach for the design of modular microfluidic systems.

This article is a PNAS Direct Submission.

[1]To whom correspondence should be addressed. Email: malmstad@usc.edu.

This article contains supporting information online at www.pnas.org/lookup/suppl/doi:10.1073/pnas.1414764111/-/DCSupplemental.

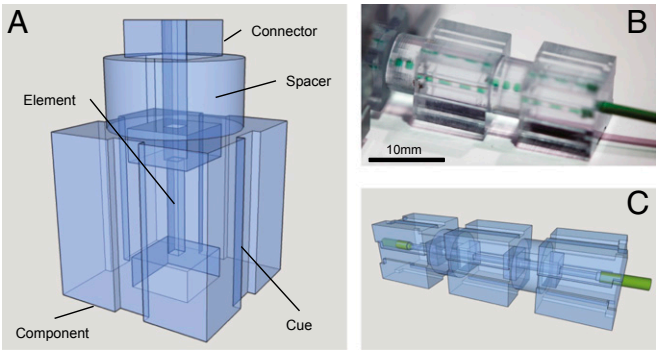

Fig. 1. (*A*) CAD assembly drawing of a 1-mm male–male connector aligned with female-type port terminating a 750-μm microfluidic element of straight pass type. (*B*) The flat mating surfaces of the connector pin and port allow for easy optical inspection of the connector–element channel junction. (*C*) Chip-to-world interfacing is performed through a single component that reversibly seals to standardized 1/16″ PEEK tubing.

process (9, 14, 15), the powerful analysis techniques used in electronics design have not been widely adopted by the microfluidics community largely due to the lack of a standardized parts platform for circuit construction, inhibiting the exploration of large-scale designs and the growth of the field in general. In other words, the advent of discrete microfluidic components with standardized interconnects and dimensional freedom naturally fits within the framework of design based on well-defined device terminal characteristics. Recently, additive manufacturing techniques such as high-resolution stereolithography have been demonstrated as effective tools for the rapid manufacturing of integrated microfluidic systems without need for a clean room (16, 17). Designers can now create complex channel networks in three dimensions and choose from a wide selection of material properties, but the cost and time involved in fabricating a single design iteration is still very high. A simpler approach would be to batch manufacture a variety of primitive elements from which a designer can assemble a functional microfluidic system. The iterative process then becomes one of immediate gratification in that the designer can quickly modify an assembly in response to fundamental design error or replace a component in order to optimize operation. The devices presented in this report take advantage of these new manufacturing approaches to produce discrete microfluidic elements with a rich variety of terminal hydrodynamic characteristics and integrated electronics for in situ process monitoring. Additive manufacturing allows the components to be made with high yields, low waste, and high resolution in three dimensions, enabling the development of an interconnect system that is not dependent on planar circuit layout.

We demonstrate an overall system development strategy that closely mimics the one used in board-level electronic circuit design and production. Analysis of pressure–flow relationships within microfluidic circuits is simplified using network analysis based on cataloged component terminal characteristics. System fabrication is reduced to a hands-on practice similar to assembling Lego bricks and aided by descriptive visual cues on each component in analogy to markings found in standardized electronic parts. Postassembly system verification involves running test flows, optimizing operating conditions, and repairing or modifying the assembly and design accordingly. Active process monitor data are communicated to a computer through a simple microcontroller. Systems can be permanently sealed by application of adhesives to the joints or potting the circuit in its entirety.

Design Concept

The fluidic components presented herein were primarily designed to contain the microfluidic elements most commonly used to perform passive fluid operations, such as junctions, mixers, splitters, and chip-to-world interfaces. All components containing functional elements were built to a standard, cubic geometric footprint (1-cm side length) and interconnect solution (Fig. 1), which lends itself easily to 3D system configuration. Inlet and outlet elements were designed to snuggly fit widely available 1/16” o.d. tubing to allow users to interface with their devices without having to commit to a proprietary chip-to-world interconnect solution. The exterior faces of each component were marked with symbolic cues that correspond to the orientation and type of element within, aiding in rapid assembly based on diagrammatic expression of the intended system. This is similar to the use of orientation marks on the packaging of fundamental discrete electronic components such as resistors, capacitors, inductors, and diodes.

Elements were terminated on component faces by female-style ports that fit a male-male style connector by means of an elastic reversible seal, enabling plug-and-play operation and reconfiguration of circuits. The female ports, corresponding male connector pins, and channels themselves were built with a square shape to ensure optical clarity through their interfaces and consistent cross-sectional channel orientation between element and connector channels. The seating of connector pins in ports was designed to ensure self-alignment and continuity between channels (Fig. S1). Unlike jumper-cable-style interconnects, connectors of this style will not lead to an accumulation of particles or increase requirements for sample volumes by breaking circuit routing out of a microfluidic environment. Connector channels, designed to have 1 mm in side length, are larger than the element channels, typically designed with 500- to 750-μm side length (Tables S1 and S2), to limit their contribution to hydrodynamic resistance while ensuring low Reynolds number flow. Connectors have a spacer between pins to alleviate difficulties in connecting and disconnecting them from components by hand. The spacers are cylindrical, and serve as lenses that optically magnify the appearance of flows and aid in postassembly test and inspection.

The library of components is shown in Table S3; their terminal hydrodynamic properties are given in Table S1. The hydraulic resistance of each element was calculated for use in circuit analysis assuming low Reynolds number flow, and varied by either modulating the cross-sectional side length of the channel or the length of the channel segment packed into the component. Each element was designed using straight channel segments with

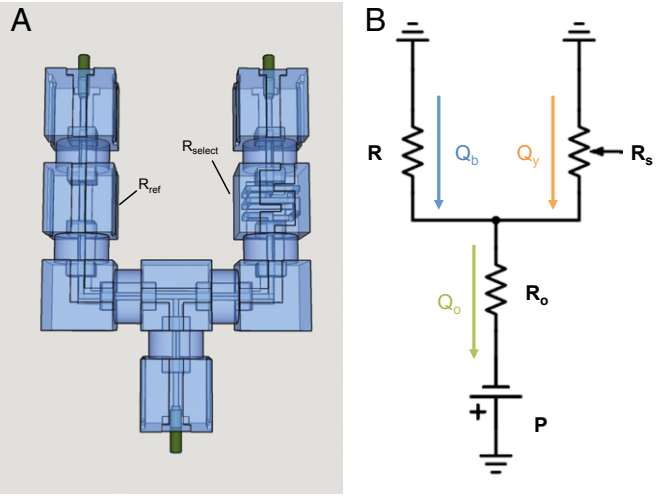

Fig. 2. (*A*) CAD assembly drawing for a 2-input, 1-output concentration gradient generator in which a single branch resistor varies the mixing ratio ($R_{select} = R_{M,750}$ as shown, see Table S1 for explanation of nomenclature and channel sizes). (*B*) Equivalent circuit diagram where R is the equivalent branch resistance compared with R_s, which is inclusive of control resistor R_{select} and additional resistance due to structural components such as interface, connector, and T-junction components.

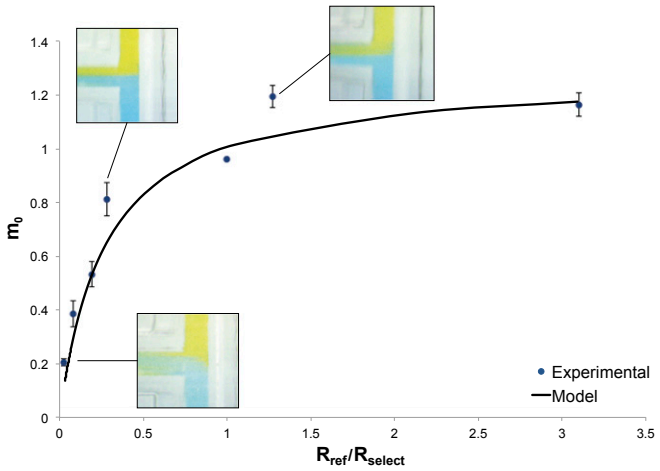

Fig. 3. Comparison of experimental and theoretical mixing ratios for a variety of R_{select} values (error bars represent the SD over 12 measurements). *Insets* show the coflowing streams at the T junction; the ratio of stream widths was used to find the output mixing ratio m_o.

square cross sections such that the net resistance for geometrically complex two-port devices (e.g., helically shaped mixers) could be computed from series addition of internal resistances. The resistances of segments themselves were calculated using Eq. **1**, derived from the solution to the Navier–Stokes equation for Poiseuille Flow in straight channels (18).

$$R_{hyd} = \frac{28.4\eta L}{h^4}. \qquad [1]$$

Here, η is the dynamic viscosity of pure water at room temperature (1 mPa·s), L is the length of a segment, and h is the height or width of the (square cross section) channel. To determine the approximate resistance of our components to use in further network analysis of assembled circuits, we optically measured the average cross-sectional side length of several channels (Table S2) and determined their variation from designed values. The expected resistance and tolerance (Table S1) for each element associated with these values was found to deviate within a range comparable to that of standard discrete electronic resistors. For elements with more than two ports, an equivalent internal circuit model was constructed, and the internal segment resistance is stated explicitly.

Tunable Mixing Through Flow Rate Division

We gauged the accuracy of our resistance calculations by constructing a parallel circuit that compares disparate branch flow rates due to a constant pressure source. The assembly described in Fig. 2 was modeled as an equivalent circuit consisting of two branch resistors R and R_s grounded by two dyed water reservoirs and terminated by outlet resistor R_o. Each branch was designed to differ by only a reference and selected component resistance, R_{ref} and R_{select}, while having identical support components resulting in equal structural resistance R_{struct}. The volumetric mixing ratio m_o of dye streams combined in the outlet resistor was predicted by nodal analysis (see *SI Text*, *Note S2*) to have simple dependency on only the selected, reference, and branch structural resistances (Eq. **2**).

$$m_o = \frac{Q_y}{Q_b} = \frac{R_{struct} + R_{ref}}{R_{struct} + R_{select}}. \qquad [2]$$

The method of Park and coworkers (19) was adapted to measure several mixing ratios with varying R_{select} and compared with theoretical values calculated from Eq. **2**, validating our model with good agreement (Fig. 3). Briefly, the resident widths of unmixed collinear dye streams were measured optically in the junction before diffusive mixing could occur. Assuming that the two dyed water streams have equal dynamic viscosity, the ratio of their

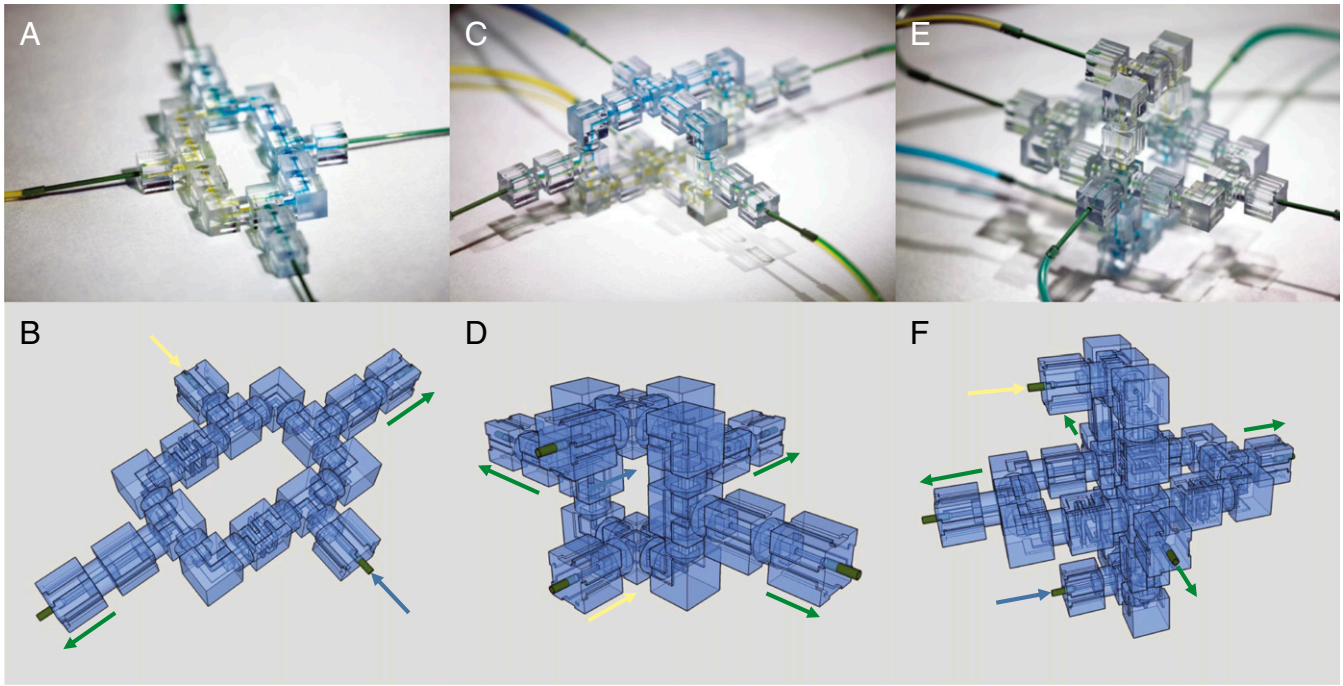

Fig. 4. Single-outlet subcircuits were combined to parallelize operation of the tunable mixer to have (*A* and *B*) two, (*C* and *D*) three, and (*E* and *F*) four outlets. Each subcircuit is constructed identically and arranged around a single inlet splitter such that the mixing ratio at each outlet is independently controlled by corresponding choices of reference and select resistors.

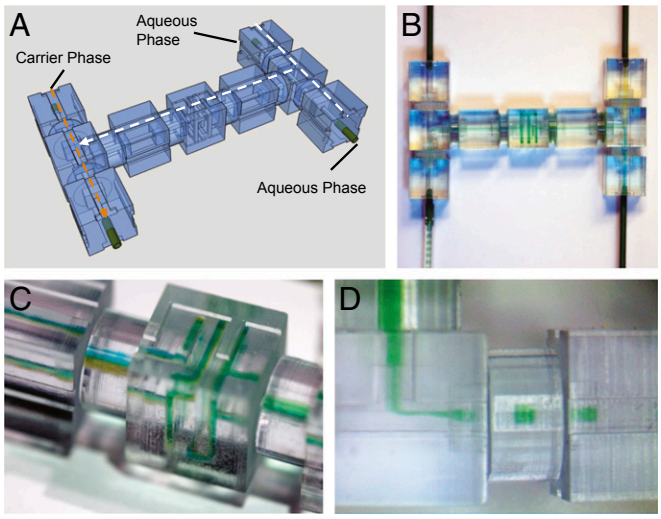

Fig. 5. (*A*) CAD assembly drawing and (*B* and *C*) realization of a T-junction configuration emulsification device. (*C*) Two dye-bearing water streams are mixed in a 3D helical mixer and (*D*) formed into microdroplets by shearing in a carrier oil phase. As shown, all connectors are 1 mm and all fluidic elements are 750 μm in cross-sectional side length.

resident widths is then directly proportional to their flow rates and thus the resistances of their originating branches.

With the ability to quickly modify the assembly, this circuit becomes a useful tool for generating precise mixing ratios based on comparison of select and reference component resistances. As seen in Fig. 4, we expanded on the operational principles of this circuit by using it as a module in two-, three-, and four-outlet large-scale tunable mixers by adding or replacing T, X, and XT junctions near the reservoir inlets. In this manner, the symmetry of the device around a single axis through which input streams were split was maintained such that the structural resistance in each new single-outlet subcircuit was unchanged between configurations. In a planar setting, this control over parallelization of operation would be impossible due to the need for extra structural components to connect these subcircuits to the inlets. By driving this circuit with a constant pressure source, each subcircuit can be analyzed as a unit with a mixing ratio that is independently controlled by its corresponding branch resistance ratio, as seen in the equivalent circuit diagrams in Fig. S2.

Reconfigurable Microdroplet Generator

In addition to being straightforward to analyze in terms of element-by-element hydrodynamics, modular microfluidic systems offer the advantage of simple reconfigurability. We demonstrate the ability to rapidly assemble and modify two common microfluidic circuit topologies used to generate droplets: T junction and flow focus (see ref. 20 for a review of these methods). In the T-junction configuration seen in Fig. 5, a single syringe pump was used to drive two dye-bearing water streams into the circuit where they were combined, mixed, and emulsified in a carrier oil stream. The helical mixer component was observed to lose effectiveness at aqueous flow rates above 2.5 $mL{\cdot}h^{-1}$, determining the upper bound for the aqueous phase subcircuit operation. The carrier phase flow rate was held constant at 1 $mL{\cdot}h^{-1}$ while the aqueous phase flow rate was varied, resulting in well-defined steady-state control of droplet size down to submillimeter sizes. As seen in Fig. 6, a 3D quad-outlet version of the T-junction subcircuit was constructed to parallelize operation for high-throughput applications. The carrier and aqueous phases were each split into four streams with cylindrical symmetry around an inlet axis through which they were introduced. Each new stream was radially transported away from the axis, and intersected with its immiscible counterpart in T junctions arranged around the axis. This "equal path-length distribution" method is similar to that demonstrated in parallelizing operation of the tuneable mixer circuit described in *Tunable Mixing Through Flow Rate Division*. The potential to produce even smaller droplets while leveraging the ability to construct 3D systems was demonstrated by replacing the T-junction subcircuit with a flow-focus subcircuit (Fig. 7). The input carrier stream assembly was built around the aqueous phase flow axis such that carrier phase was transported vertically down into an X junction where droplets were formed. The aqueous phase flow rate was varied once again and the carrier phase flow rate was raised to 5 $mL{\cdot}h^{-1}$ to prevent droplet coalescence in the connector channels near the outlet. The center-channel length of the droplets outside of the device produced by both circuits was measured optically and shown to reliably depend on the ratio of aqueous and carrier phase flow rates (Fig. 8).

In Situ Monitoring of Droplet Production

Active elements can be incorporated into the modular packaging described here by building sensors and actuators into the stereolithographically fabricated parts. Here, we demonstrate the incorporation of an off-the-shelf near-infrared emitter–receiver pair into a component designed for droplet sensing (Fig. 9). The component was designed such that the diodes fit snugly into embossed features on the exterior, creating a beam path that intersects a straight pass channel element (Fig. 9*A*). The channel carries water droplets dispersed in a fluorocarbon oil phase formed by an upstream T-junction circuit. The voltage signal across the phototransistor detector biased in saturation mode is monitored (Fig. S3). As droplets of water cross the beam, they absorb the near-infrared light much more than the carrier oil. The resulting signal (Fig. 9*C*) is digitized and communicated to a PC by a microcontroller to determine the droplet production frequency. The length of the droplets was deduced from the average flow velocity in the channel and half-period of the signal (i.e., the droplet residence time in the beam), and compared directly with droplet sizes measured by optical microscopy. Our results show good agreement between the two techniques and suggest that by incorporating more market-available discrete electronic

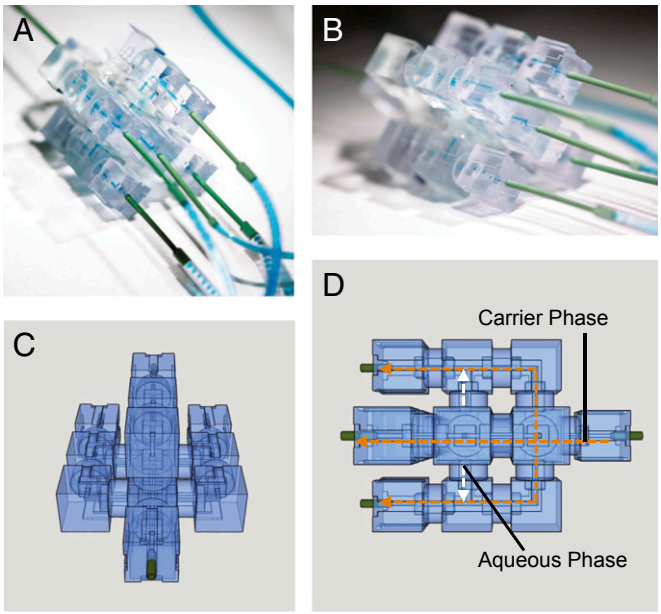

Fig. 6. (*A* and *B*) Realization and (*C* and *D*) CAD assembly drawings of a high-throughput T-junction configuration subcircuit built in three dimensions. As shown, the channel cross-sectional side length for all connectors is 1 mm and for all fluidic elements is 750 μm.

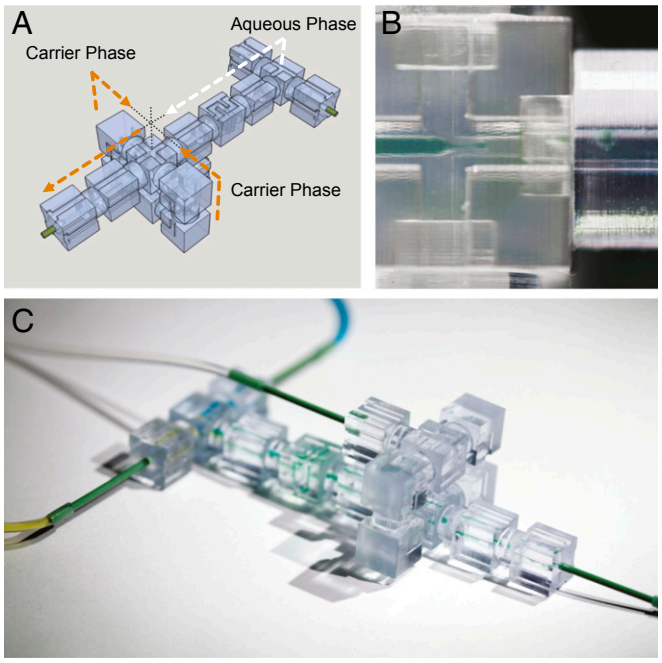

Fig. 7. (*A*) CAD assembly drawing and (*B* and *C*) realization of a flow-focus configuration emulsification device constructed by replacing a terminal T-junction subcircuit with an X-junction-based module in which the flow focusing is performed. As shown, the channel cross-sectional side length for all connectors is 1 mm and for all fluidic elements is 750 μm.

devices into our components, active process monitoring and feedback control systems can be implemented with ease.

Assembly and Postprocessing

The material and geometries selected for components and connectors demonstrated excellent wear resistance. The T-junction emulsification circuit described above was completely disassembled, reassembled, operated, and cleaned in 28 sequential trials without any leakage. The first two or three times a connector was attached to a component, removing it was difficult by hand due to the tight tolerance associated with the connector seating but could be accomplished by inserting a razor blade at the joint underneath the spacer and gently prying it loose. Fresh joints between components and connectors showed no signs of leakage under flow rates as high as 200 $mL{\cdot}h^{-1}$. Leaks were only observed in connectors where the pin edges had been chipped during rough disassembly.

We explored modifying the surface properties of the channels by coating them with a fluoropolymer coating via a vapor-phase technique we have previously demonstrated for modifying channels in poly(dimethylsiloxane) (PDMS) devices (21, 22). In brief, initiated chemical vapor deposition (iCVD) was used to coat the channels in stereolithographically fabricated components with poly(1H,1H,2H,2H-perfluorodecyl acrylate-co-ethylene glycol diacrylate), making the channel walls hydrophobic and increasing the contact angle of a water droplet in oil from 67.9° to 138.3° (Fig. S4). The coating did not affect the optical clarity of the photoresin material.

In addition to reversible assembly techniques, we explored several approaches to permanently sealing the system for applications where further mechanical, thermal, or chemical durability is required. Connector–component joints can be sealed with either fast-curing epoxy or silicone pipe sealant via direct application with a cotton-tipped applicator. A microfluidic circuit was also potted by connecting interface components to breather tubes, completely immersing the assembly in PDMS, and curing it at 30 °C for 24 h. The results of these permanent sealing approaches are shown in Fig. S5.

Discussion

We have demonstrated a robust solution for the rapid benchtop assembly of 3D microfluidic systems from a library of standardized discrete elements. Components were fabricated using additive manufacturing methods and characterized by their terminal flow characteristics, enabling the use of circuit theory to accurately predict the operation of a microfluidic mixing system with scalable complexity in three dimensions. The assembly time (from part selection to initial testing) for our most complex systems was less than 1 h. In addition to being much faster to prototype than monolithic devices, this system also allows for 3D configurations that were not previously possible using other modular technologies. By discretizing and standardizing the primitive elements composing such systems, newly found design complexity naturally allows for hierarchal system analysis techniques borrowed from the hydraulic analogy to electronic circuit design. This in turn allows the designer to have greater focus on satisfying a dynamic set of operational load requirements rather than working within the restrictively static environment of planar manufacturing.

The ability to reconfigure our systems toward expanded operational capabilities was further demonstrated by attaching three emulsification subcircuit modules to a simple mixing circuit to form droplets over a wide range of volumes and generation rates. Despite less need for analytically predictable operation, piecewise validation was also shown for these canonical two-phase flow systems by qualifying the mixer subcircuits and then in turn the emulsifier subcircuits for functionality. In a monolithic device, each of the circuits demonstrated would comprise a single system prone to complete failure due to singular manufacturing error or design error of a single element. In our system, components in circuit assembly were quickly assessed for their independent contribution to failure and replaced or modified accordingly. Only after successful test and validation were devices optionally

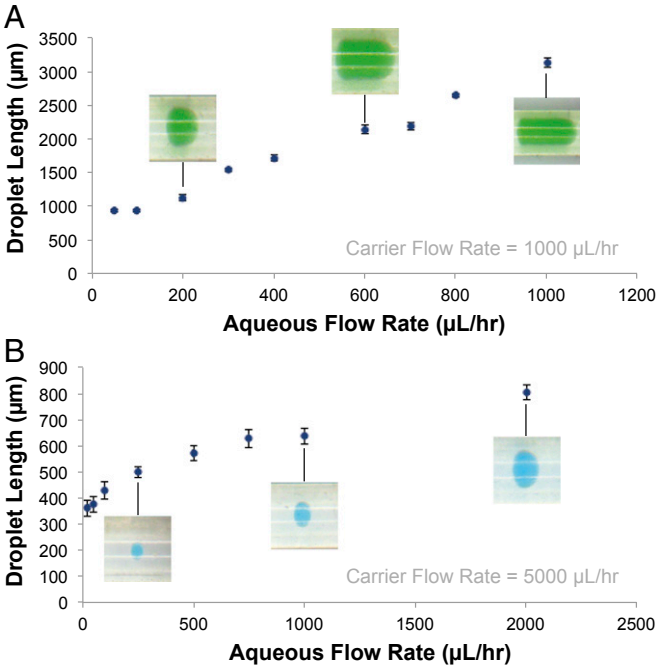

Fig. 8. Droplet length as measured along the center axis of exit tubing for (*A*) T-junction and (*B*) flow-focus circuit subsystems terminating a two-stream mixer circuit (error bars represent SD over 12 measurements). Note that the flow-focused system allows a smaller droplet size regime to be obtained despite maintaining equivalent fluid element geometries: The channel cross-sectional side length is 1 mm for all connectors and 750 μm for all fluidic elements. *Insets* are selected examples of images collected to determine the monodispersity and average values of droplet size distributions.

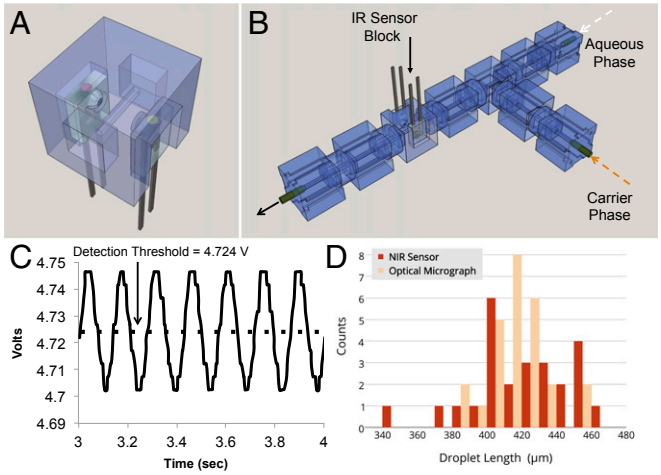

Fig. 9. (*A*) CAD representation of a component with a straight pass channel of 642.5-μm cross-sectional side length intersecting the beam created between a discrete near-infrared (NIR) diode emitter and phototransistor receiver. (*B*) The component is placed downstream from a T junction producing water-in-oil droplets that absorb the beam as they cross its path and (*C*) generating a periodic signal at the output of the detector. (*D*) The residence time of the droplets in the beam and the average velocity of the droplet train are used to calculate a distribution of droplet lengths, which are compared directly to measurements taken using standard optical microscopy techniques. Flow rates were set to 5,000 $\mu L \cdot h^{-1}$ and 2,000 $\mu L \cdot h^{-1}$ for the carrier and aqueous phases, respectively. Droplet lengths were determined to be 421.22 μm + 27.54 μm and 416.90 μm + 16.36 μm by the NIR sensor and optical micrographs, respectively.

sealed into permanent configurations while maintaining their optical clarity and ease of interfacing.

The operational performance of one of these circuits was also successfully monitored by inclusion of a single active component capable of performing in situ sensing. This implies that the ability to reconfigure our system is also advantageous from the standpoint of metering systems before finalization of a design. In addition, the inclusion of active sensing components is particularly advantageous when considering process monitoring in highly complex systems with many subcircuits: Densely routed microfluidic systems do not integrate well into standard analysis tools such as optical microscopes.

We envision that this system can make discrete microfluidics a valuable development vehicle for complex design that has not yet been achieved. With a wider library of passive and active components to choose from, this system can replace monolithically integrated devices for many microfluidic applications. In addition, this system will benefit immensely as industrial additive manufacturing technologies also improve, allowing for the further miniaturization of elements and development of an even larger selection of elements and materials.

Materials and Methods

Channels in the microfluidic elements have square cross sections of side lengths 500 μm, 635 μm, 750 μm, and 1,000 μm. Channels passing through the connectors have a side length of 1,000 μm. The 1/16 inch-o.d. polyether ether ketone (PEEK) tubing was used to interface with inlet and outlet components in all circuits. In all droplet studies, flow was driven by Harvard Apparatus 2200 syringe pumps, assemblies were constructed using h = 750 μm components, and Halocarbon 4.2 oil was used as a carrier phase. Droplets were measured in 1/16" i.d. silicone tubing exterior of the assembly. Components were cleaned between use by flushing their channels with water, soaking them in isopropanol for 10 min, and drying them with pressurized air. All components were designed using SketchUp 2013 (Trimble Ltd.) computer-aided design (CAD) software and exported into .stl format in preparation for production using a community-provided software extension. Manufacturing was performed by FineLine Prototyping, Inc., using a stereolithographic process and Somos WaterShed XC 11122 photoresin (16). Near-infrared process monitoring was accomplished using a SEN-00241 940-nm, 75-mW Emitter/Detector kit and Arduino Mega microcontroller development board. Data were communicated directly over USB to a PC and processed off-controller in real time using Mathworks MATLAB R2014a. Devcon Home 5 Minute Epoxy and Permatex Silicone RTV Adhesive were both used to seal component joints for permanent configuration of devices. A thin layer of 5 Minute Epoxy was spread by hand over unfinished component surfaces with fogged or opaque appearance to enhance their optical clarity.

Nodal analysis was used to determine the volumetric mixing ratio of dye in the flow comparator circuit. Food dye in deionized water was used to visualize the resident width of each branch flow in the outlet junction. Flow in each branch was induced using a negative displacement pump built in-house. All resistors in the equivalent circuit model (Fig. 2*B*) were approximated by series addition of their contributing element resistances. Poiseuille's law was then applied to relate branch resistances to flow rates, allowing us to derive Eq. **2**. The derivation is detailed in *SI Text, Note S2*.

ACKNOWLEDGMENTS. We are grateful to Carson Riche and Dr. Malancha Gupta for performing iCVD modification of channels. Funding for this work was provided in part by the National Institutes of Health (Award 1R01GM093279).

1. Whitesides GM (2006) The origins and the future of microfluidics. *Nature* 442(7101):368–373.
2. Stone HA, Stroock AD, Ajdari A (2004) Engineering flows in small devices. *Annu Rev Fluid Mech* 36(1):381–411.
3. Manz A, Graber N, Widmer HM (1990) Miniaturized total chemical analysis systems: A novel concept for chemical sensing. *Sens Actuators B* 1(1-6):244–248.
4. Squires T, Quake S (2005) Microfluidics: Fluid physics at the nanoliter scale. *Rev Mod Phys* 77(3):977–1026.
5. Sackmann EK, Fulton AL, Beebe DJ (2014) The present and future role of microfluidics in biomedical research. *Nature* 507(7491):181–189.
6. Yuen PK (2008) SmartBuild—A truly plug-n-play modular microfluidic system. *Lab Chip* 8(8):1374–1378.
7. Shaikh KA, et al. (2005) A modular microfluidic architecture for integrated biochemical analysis. *Proc Natl Acad Sci USA* 102(28):9745–9750.
8. Miserendino S, Tai Y-C (2008) Modular microfluidic interconnects using photodefinable silicone microgaskets and MEMS O-rings. *Sens Actuators A* 143(1):7–13.
9. Sun K, Wang Z, Jiang X (2008) Modular microfluidics for gradient generation. *Lab Chip* 8(9):1536–1543.
10. Grodzinski P, Yang J, Liu RH, Ward MD (2003) A modular microfluidic system for cell preconcetration and genetic sample preparation. *Biomed Microdevices* 5(4):303–310.
11. Rhee M, Burns MA (2008) Microfluidic assembly blocks. *Lab Chip* 8(8):1365–1373.
12. Langelier SM, et al. (2011) Flexible casting of modular self-aligning microfluidic assembly blocks. *Lab Chip* 11(9):1679–1687.
13. Oh KW, Lee K, Ahn B, Furlani EP (2012) Design of pressure-driven microfluidic networks using electric circuit analogy. *Lab Chip* 12(3):515–545.
14. Lee K, et al. (2009) Microfluidic network-based combinatorial dilution device for high throughput screening and optimization. *Microfluid Nanofluid* 8(5):677–685.
15. Stiles T, et al. (2005) Hydrodynamic focusing for vacuum-pumped microfluidics. *Microfluid Nanofluid* 1(3):280–283.
16. Au AK, Lee W, Folch A (2014) Mail-order microfluidics: Evaluation of stereolithography for the production of microfluidic devices. *Lab Chip* 14(7):1294–1301.
17. Kitson PJ, Rosnes MH, Sans V, Dragone V, Cronin L (2012) Configurable 3D-printed millifluidic and microfluidic 'lab on a chip' reactionware devices. *Lab Chip* 12(18):3267–3271.
18. Bruus H (2008) *Theoretical Microfluidics,* Oxford Master Series in Condensed Matter Physics (Oxford Univ Press, Oxford), Vol 18.
19. Choi S, Lee MG, Park J-K (2010) Microfluidic parallel circuit for measurement of hydraulic resistance. *Biomicrofluidics* 4(3):1–9.
20. Teh S-Y, Lin R, Hung L-H, Lee AP (2008) Droplet microfluidics. *Lab Chip* 8(2):198–220.
21. Riche CT, Marin BC, Malmstadt N, Gupta M (2011) Vapor deposition of cross-linked fluoropolymer barrier coatings onto pre-assembled microfluidic devices. *Lab Chip* 11(18):3049–3052.
22. Riche CT, Zhang C, Gupta M, Malmstadt N (2014) Fluoropolymer surface coatings to control droplets in microfluidic devices. *Lab Chip* 14(11):1834–1841.